

# Accepted Manuscript

Influence of High Fidelity Structural Models on the Predicted Mass of Aircraft Wing Using Design Optimization

Odeh Dababneha, Timoleon Kipouros

PII: S1270-9638(18)30211-6  
DOI: <https://doi.org/10.1016/j.ast.2018.05.043>  
Reference: AESCTE 4596

To appear in: *Aerospace Science and Technology*

Received date: 27 January 2018  
Revised date: 17 April 2018  
Accepted date: 23 May 2018

Please cite this article in press as: O. Dababneha, T. Kipouros, Influence of High Fidelity Structural Models on the Predicted Mass of Aircraft Wing Using Design Optimization, *Aerosp. Sci. Technol.* (2018), <https://doi.org/10.1016/j.ast.2018.05.043>

This is a PDF file of an unedited manuscript that has been accepted for publication. As a service to our customers we are providing this early version of the manuscript. The manuscript will undergo copyediting, typesetting, and review of the resulting proof before it is published in its final form. Please note that during the production process errors may be discovered which could affect the content, and all legal disclaimers that apply to the journal pertain.



1 **Influence of High Fidelity Structural Models on the**  
2 **Predicted Mass of Aircraft Wing Using Design Optimization**

3 Odeh Dababneh<sup>a\*</sup>, Timoleon Kipouros<sup>b,c</sup>

4 <sup>a</sup>*School of Mechanical and Aerospace Engineering, Queen's University Belfast,*  
5 *Belfast, Northern Ireland BT9 5AH, United Kingdom*

6 <sup>b</sup>*Engineering Design Centre, Department of Engineering*  
7 *University of Cambridge, Cambridge, CB2 1PZ, United Kingdom*

8 <sup>c</sup>*School of Aerospace, Transport and Manufacturing*  
9 *Cranfield University, Cranfield, MK43 0AL, United Kingdom*

10

11 **Abstract**

12 This paper explores the necessary and appropriate level of detail that is required to describe the structural  
13 geometry of aircraft wings accurately enough to predict the mass of the main load-carrying wing structure  
14 to an acceptable level of accuracy. Four different models of increasing structural fidelity are used to  
15 describe the wingbox structure of a realistic real-world aircraft wing. The wingbox of the NASA  
16 Common Research Model served as a test model for exploring and analyzing the trade-off between the  
17 granularity level of the wingbox geometry description under consideration and the computational  
18 resources necessary to achieve the required degree of accuracy. The mass of metallic and composite  
19 wingbox configurations was calculated via finite element analysis and design optimization techniques.  
20 The results provided an insight into the competence of certain wingbox models in predicting the mass of  
21 the metallic and composite primary wing structures to an acceptable level of accuracy, and in  
22 demonstrating the relative merits of the wingbox structural complexity and the computational time and  
23 input efforts for achieving the required level of accuracy.

24 **Keywords:** Wing Mass; Primary Wing Structures; High-Fidelity Models; Finite Element; Optimization

25 **Nomenclature**

26	$a_{composite}$	Cross-sectional area of the composite wingbox flanges, mm <sup>2</sup>
27	$a_{metallic}$	Cross-sectional area of the metallic wingbox flanges, mm <sup>2</sup>
28	$b$	Wing semi-span, m
29	$C$	Wing chord length, m
30	$E_{11}$	Longitudinal modulus, GPa
31	$E_{12}$	Transverse modulus, GPa
32	$E$	Elastic modulus, GPa
33	$EI$	Bending stiffness
34	$FI$	Failure index

35

36 <sup>\*</sup>Corresponding author  
37 *E-mail address: odeh.da@gmail.com; o.dababneh@qub.ac.uk*

38	$G_{12}$	In-plane shear modulus, GPa
39	GJ	Torsional stiffness
40	$M(\mathbf{x})$	Objective function representing the wingbox structural mass
41	$n_{ply}$	Number of plies
42	$t_{metallic}$	Thickness of the metallic wingbox panels, mm
43	$\delta_{tip(z)}$	Z-Component of the wingtip displacement
44	$(\delta)_{max}^+$	Maximum vertical displacement in positive direction
45	$(\delta)_{max}^-$	Maximum vertical displacement in negative direction
46	$\varepsilon_{allowable}$	Allowable strain
47	$\varepsilon_{principal}$	Principal strain
48	$\theta_{tip}$	Angle of twist at the wingtip, deg
49	$\mu\varepsilon$	Micro strain
50	$\nu_{12}$	Major Poisson's ratio
51	$\sigma_{allowable}$	Allowable stress
52	$\sigma_{von Mises}$	von Mises stress
53	$\sigma_{ultimate}$	Ultimate stress
54	$\sigma_{axial}$	Axial stress

## 55 1. Introduction

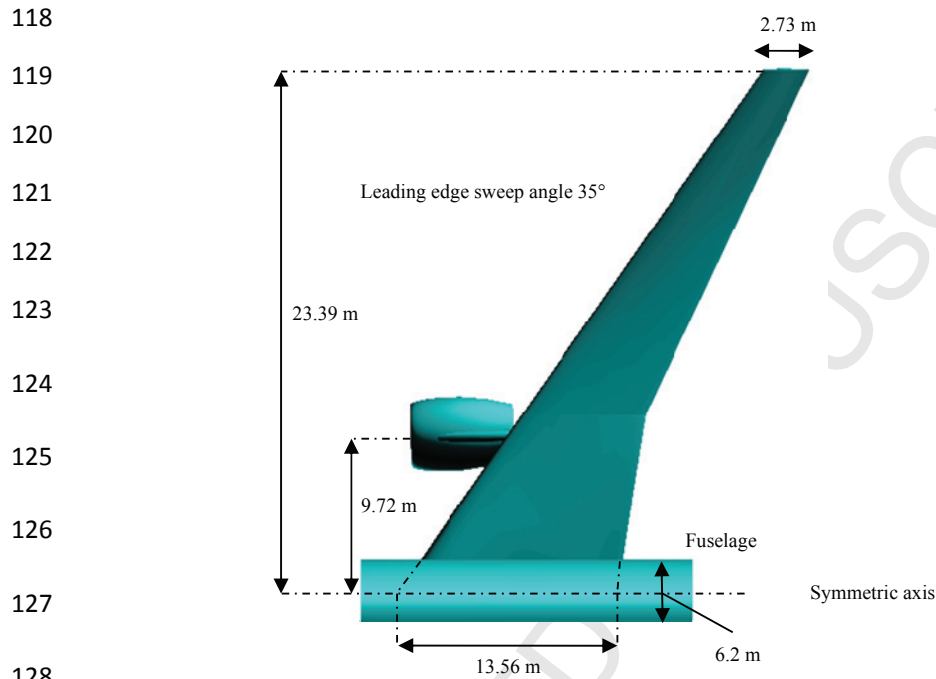
56 In a conventional approach to aircraft wing mass estimation at the early stages of the design process,  
57 wing mass property design engineers usually follow a particular published methodology, such as one of  
58 those proposed by Raymer [1], Roskam [2] or Torenbeek [3]. Taking up as much as 35-50% of the  
59 operating empty weight of modern transport aircraft [4], the wing is one of the heaviest structural  
60 components of an aircraft. In recent years, aircraft manufacturers and research institutes have been  
61 focusing on aircraft concepts that require new wing designs. The NASA Common Research Model  
62 (CRM) for a generic transport aircraft model is an example [5,6]. The design of an efficient aircraft wing  
63 featuring new technologies has always represented a substantial challenge for aircraft designers,  
64 especially when the proposed novel concept challenges the existing knowledge base and the accuracy of  
65 normally used empirical methods and statistical data collected from previously constructed aircraft. These  
66 methods are generally limited to conventional aircraft designs constructed from light metallic alloys and  
67 are unable to assess the relative benefits of novel wing design concepts as well as advanced materials,  
68 such as composite materials. In the literature, great efforts have been put into and reported on developing  
69 and classifying wing mass prediction methods [7-10]. This is because of the well-defined structural role  
70 of the wingbox as a primary load-carrying component and the importance of optimum wing design as a  
71 significant subject of the preliminary design phase [11]. The open literature on the subject of wing mass  
72 estimation methods and their applications in the aerospace industry has been comprehensively discussed  
73 by Dababneh and Kipouros in [12]. In their work, the current state of the art of aircraft wing mass  
74 estimation methods has been reviewed. Special attention has been given to classifications of wing mass

75 estimation methods and to the current challenges and technological difficulties in wing mass estimation  
76 methods. According to [12], determining the mass of an aircraft wing, for which the database is  
77 insufficient or non-existent or the wing design lies beyond the use of empirical methods, via fully  
78 integrated finite element analysis [13-17], and design optimization methods [18,19,20] appears to be a  
79 promising approach to consider at the early stages of the design process. This has been made possible  
80 over the last 10 years by the increased processing power of computers, the advancements in computer-  
81 aided design, the enhancement of multi-dimensional design space visualizations, simultaneous  
82 calculation, visual screening and representations of a variety of design analysis and optimization results  
83 [21]. With design optimization, one is usually concerned with the chosen form of the structural model and  
84 the finite element level of detail in the wingbox that is needed to be considered in order to achieve the  
85 required results. Ciampa et al. [22] highlighted the importance of significantly reduced complexity finite  
86 element models in the pre-design phase process of aircraft wing structures. In their work, they showed  
87 that the wing skin stiffened panels can be represented by stiffness-equivalent panels. This procedure  
88 enables a fast search for an optimum mass with low computational resources, but does not provide  
89 enough information for the sizing of stiffened panels. In another example, Yang et al. [23], revealed that  
90 adequate natural frequency and mode shape results for a complex wing structure can be achieved by using  
91 an equivalent wing model, in which each wing segment is modeled as equivalent plate, reducing the wing  
92 structural complexity to a simple model and hence the cost of the design task. In the field of structural  
93 design optimization concepts for aerospace industry, Ritter [24] showed that while the industry-standard  
94 beam-rod representation of aircraft wing is sufficient for linear aeroelastic simulations, a 3D wingbox  
95 model, which resembles a real aircraft wing much more realistically, will provide valuable insight into the  
96 aeroelastic dynamic behavior of the structure especially when the design optimization process is focused  
97 on aeroelastic tailoring [25]. The scope of this study is to investigate and understand the effect of using  
98 different wingbox configurations of increasing structural complexity on the mass estimation of the wing  
99 primary structure. The goals of the present study are mainly twofold. The first is to identify and select an  
100 appropriate model that can predict the mass of the CRM wingbox to an acceptable level of accuracy. It  
101 also has to allow the designer to explore and assess the design decisions made, such as the choice of  
102 construction material, at an early stage of the design process, thus eliminating any costly changes during  
103 the detailed design process, and can serve as well as a baseline model for future complex structural  
104 optimization studies. The second is to demonstrate the trade-off between the wingbox structural  
105 complexity models under consideration and the user input efforts and computational time needed to  
106 achieve sufficiently accurate results for the intended design and analysis purposes.

## 107 2. Technical description of the CRM wing

108 The CRM is a modern single-aisle transport-class aircraft configuration that was generated as an open  
109 geometry for collaborative research within the aerodynamics community. It has a wingspan of 58.76 m, a  
110 mean aerodynamic chord of 7.0 m, an aspect ratio of 9.0, a taper ratio of 0.275, a leading edge sweep  
111 angle of 35°, a break along the trailing edge at 37% of the semi-span (also referred to as the yehudi  
112 break), a wing tip chord of 2.73 m, a wing root chord of 13.56 m and a cruise Mach number of 0.85. The

113 maximum take-off mass (MTOM) is set to 260,000 kg. The maximum cruise speed limit is set to  $V_C =$   
 114 193 m/s EAS with a cruise Mach number of  $M_C = 0.85$ . The dive speed is set to  $V_D = 221.7$  m/s EAS with  
 115 a dive Mach number of  $M_D = 0.92$ , which results from the equation  $M_D = M_C + 0.07$  given in [26]. The  
 116 cruise altitude is taken as 10,668 m. The planform of the wing and the relevant data are presented in Fig.  
 117 2.



129 **Fig. 2** Planform of the CRM wing

### 130 3. Structural and finite element modeling of the CRM wing

131 The CRM primary wing structure is modeled to meet the minimum design requirements set forth in  
 132 the Federal Aviation Regulations (FAR) Part 25 [27] and/or the European Aviation Safety Agency  
 133 (EASA) CS-25 [26]. Traditional two-spar wingbox architecture is used as a baseline design. The external  
 134 geometry is defined by CRM.65-BTE airfoil sections and the wingbox is derived from the wing surface  
 135 model by defining the front and rear spar positions at 12% and 71% of the local airfoil chord. The internal  
 136 layout is defined by the stiffener pitch, rib pitch and orientation based on the values for a typical large  
 137 transport aircraft wing. Fig. 3 shows the CRM wing surface model and the wingbox derived from it.

138

139

140

141

142

143

144

145

146

147

148

149

150

151

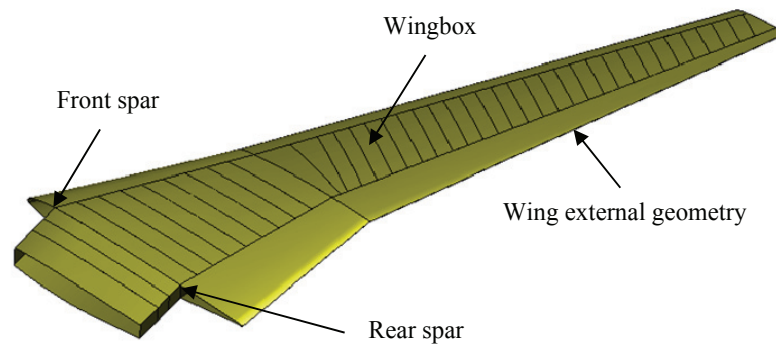


Fig. 3 Surface and wingbox model of the CRM wing

### 152 3.1 Description of the considered structural models

153 The main load carrying wing structure is created using different models of increasing structural  
 154 fidelity, as shown in Figs. 4-7. The main goal is to identify and select an appropriate model that can  
 155 predict the mass of the primary wing structure to an acceptable level of accuracy. This done by  
 156 conducting comparative effectiveness studies that aim to investigate the effects of using different  
 157 wingbox configurations on the definition of the analysis and optimization models, and therefore on the  
 158 wingbox mass estimation.

#### 159 1. Wingbox section model 1

160 In this model, as shown in Fig. 4, each bay in the wingbox is modeled by four un-stiffened thin-walled  
 161 panels. These panels represent the upper and lower skins of the wingbox, as well as the front and rear spar  
 162 webs. The thicknesses of the panels are treated as independent design variables representing the wing  
 163 torsion box and contributing to bending strength properties.

164

165

166

167

168

169

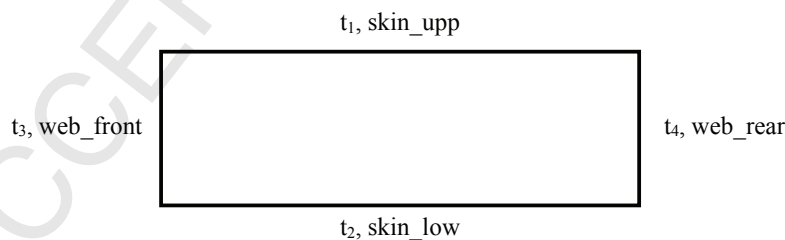
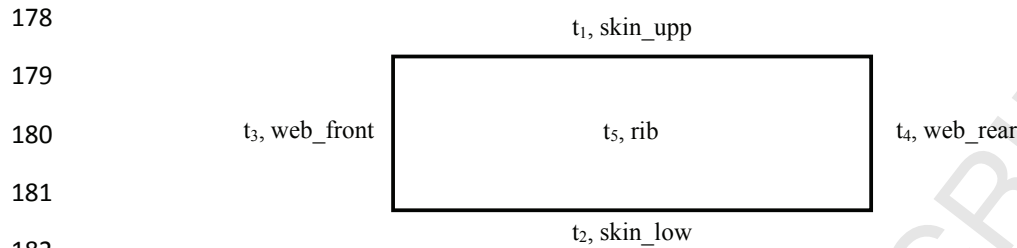


Fig. 4 Wingbox section Model 1 and related design parameters

#### 170 2. Wingbox section model 2

171 This model, as shown in Fig. 5, retraces the previous one and considers the rib thickness as a fifth  
 172 independent design variable. The number of ribs and their spacing is determined from previously acquired  
 173 knowledge and evidence from other engineering designs. The ribs and their spacing must maintain the  
 174 aerodynamic shape of the wing and provide enough clearance through the access hole between each rib

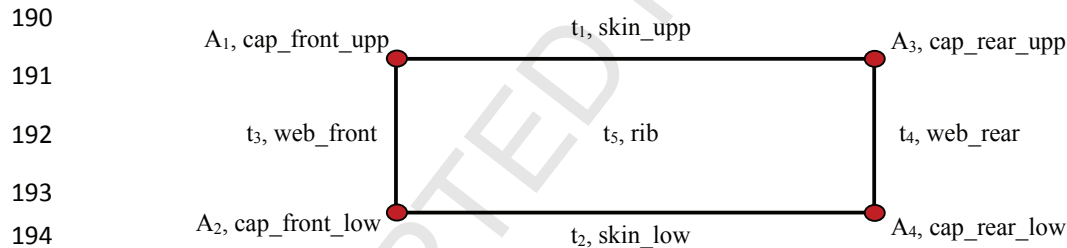
175 section for inspections and maintenance throughout the operational life of the aircraft. A better evaluation  
 176 and understanding of the wingbox in-plane and out-of-plane stiffness and bending requirements is hoped  
 177 to be gained using this model.



183 **Fig. 5** Wingbox section Model 2 and related design parameters

### 184 3. Wingbox section model 3

185 Four additional independent design variables are added to the third model: upper and lower spar caps  
 186 are added to the front and rear spars, as illustrated in Fig. 6. The spar caps take most of the loads from the  
 187 bending moments, and due to the presence of the spar web, one cap experiences a tension force while  
 188 another undergoes compression. The spar caps' cross-sectional areas are usually large and vary along the  
 189 wing.



195 **Fig. 6** Wingbox section Model 3 and related design parameters

### 196 4. Wingbox section model 4

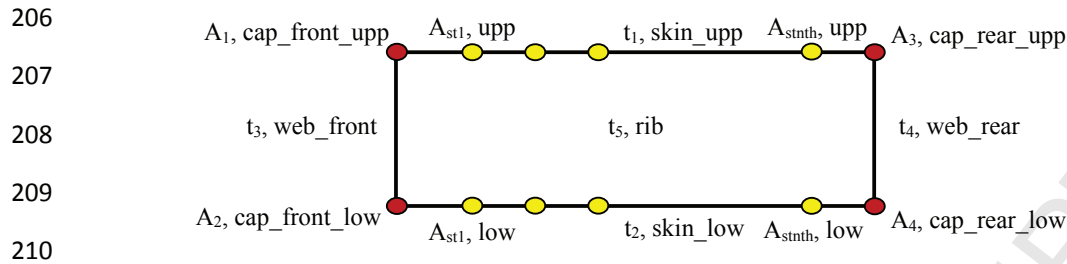
197 Stiffeners are added as new independent design variables to the previous model, as shown in Fig. 6.  
 198 They are used to support the skin between the ribs and to account for the instability of the thin-walled  
 199 panels. The stiffeners are also used to resist the part of the bending moment which is not resisted by the  
 200 spar caps and to take some of the tension and compression loads with effective skin areas. The number of  
 201 stiffeners and the distance between them is determined from previous design experience.

202

203

204

205



211 **Fig. 7** Wingbox section Model 4 and related design parameters

212 The wingbox of the CRM aircraft is designed by considering both metallic and composite materials,  
 213 which have a high strength-to-weight ratio for lightweight structures, high strength and stiffness  
 214 properties, good fatigue and corrosion resistance. High-strength aluminum 7050-T7451 alloy [28] is used  
 215 for the design of the upper skins, upper stringers and spar caps of the wingbox, and 2024-T351 alloy [29]  
 216 is used for the design of the lower skins, lower stringers and the ribs, since it is better suited for structures  
 217 stressed by cyclic tension loads and therefore prone to fatigue damage. In addition to aluminium alloys,  
 218 composite materials made up of T300 carbon fibres and N5208 epoxy resin, which is widely used in the  
 219 aircraft industry, is used as a second material choice for the wingbox structure design [30]. For modeling  
 220 the wingbox using a composite material, a symmetric and balanced laminate with ply orientation angles  
 221 of [45/0/-45/90]s was created in order to get an orthotropic material. The aim of this design procedure  
 222 was to avoid shear extension and membrane bending coupled behaviors.

### 223 3.2 Aerodynamic loads calculation of the CRM wing

224 For the CRM wing, the design loads are obtained from two scenarios, related to flight maneuvers and  
 225 gust conditions, in accordance with the standard airworthiness certification regulations [26,27]:

- 226 1. Symmetric pull-up maneuver load for the maximum positive limit load factor at maximum take-  
 227 off mass and maximum dive speed,  $V_D$ , at sea-level standard atmospheric conditions;
- 228 2. Gust loads for the maximum gust load factor at maximum zero fuel mass and maximum cruise  
 229 speed,  $V_C$ , at a critical gust altitude of 6,100 m.

230 The symmetric pull-up maneuver at the limit load factor ( $n = 2.5$ ) at maximum take-off mass (260,000  
 231 kg) and design dive speed ( $V_D = 221.7$  m/s EAS,  $M_D = 0.65$ ) at sea-level conditions was found to be the  
 232 critical one for the design, analysis and sizing optimization of the CRM wingbox and hence the mass  
 233 estimation. There are currently several theoretical methods available for determining the aerodynamic  
 234 loading of an aircraft wing. Many of the theoretical solutions have been programmed for digital  
 235 computation, and separate computer programs have been used to calculate the aerodynamic forces on an  
 236 aircraft wing in different flow conditions. The choice of the appropriate method depends on the  
 237 complexity of the aircraft wing, the purpose of the analysis, the computational cost and the level of  
 238 accuracy required at the design stage. In the current study, the spanwise lift force and pitching moment  
 239 were calculated using the ESDU 95010 computer program. ESDUpac A9510 utilizes steady lifting-  
 240 surface theory based on the Multhopp-Richardson solution to calculate the spanwise loading of wings

241 with camber and twist in subsonic attached flow [31]. Figs. 8 and 9 give the local overall lift and pitching  
 242 moment coefficients calculated about a local quarter chord.

243

244

245

246

247

248

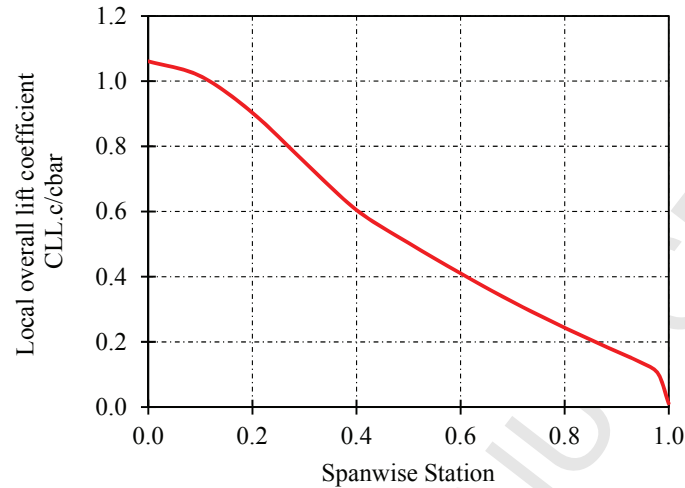
249

250

251

252

253



254 **Fig. 8** Spanwise local overall lift coefficient

255

256

257

258

259

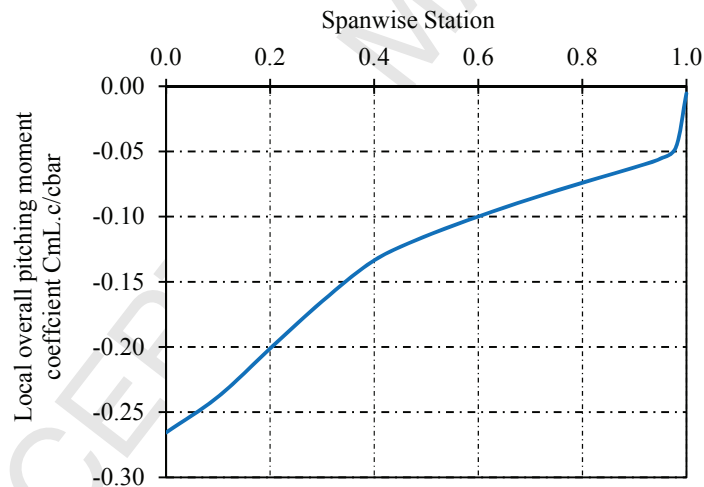
260

261

262

263

264

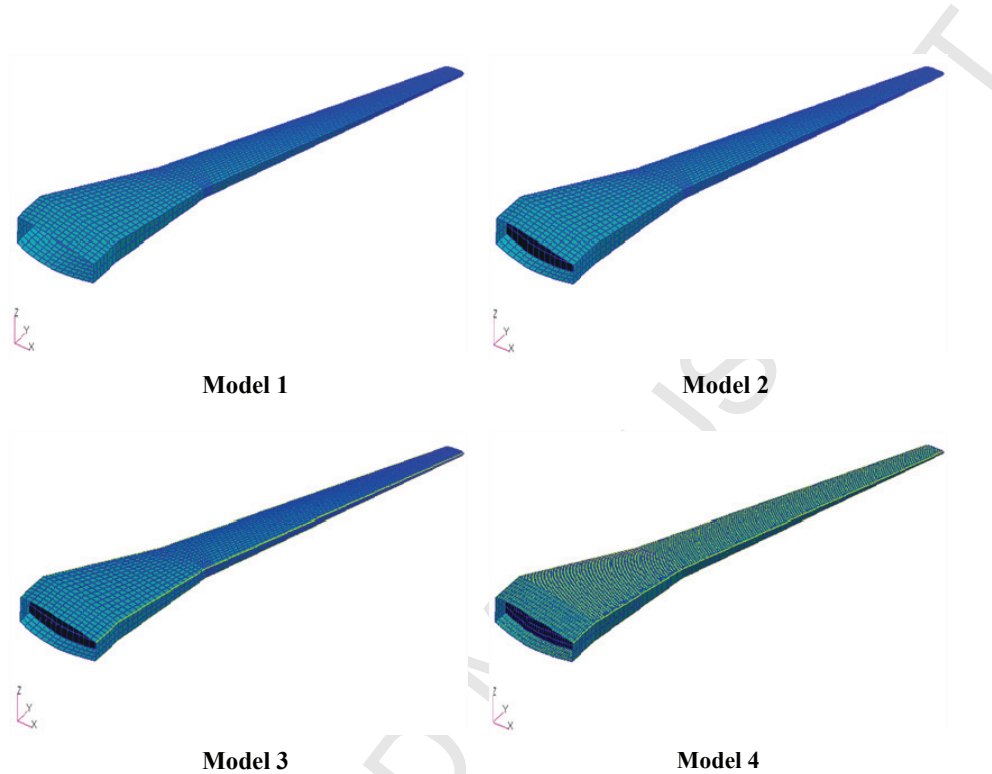


265 **Fig. 9** Spanwise local overall pitching moment coefficient

### 266 3.3 Finite element modeling of the CRM wing

267 In the current study, the thin-walled structures of the CRM wingbox configurations (skins, webs and  
 268 ribs) were modeled using two-dimensional quadrilateral and triangular shell elements (CQUAD4,  
 269 CTRAI3) with in-plane membrane and bending stiffness. On the other hand, stringers and spar caps were  
 270 modeled using one-dimensional rod elements (CROD) with axial stiffness. Finite element models of the  
 271 CRM wingbox configurations are generated using MSC Patran, based on the physical dimensions and  
 material properties of the structural cross-sectional models as specified in section 3 The wing platform

272 was modeled for a half-wing section. The structure within the leading and trailing edges was not modeled  
 273 and the lower skin of the wing has no manholes. Fig. 10 shows the finite element mesh models for the  
 274 CRM wingbox structures.



275

276

**Fig. 11** Finite element mesh models of the CRM wingbox structures-Models 1-4

277 The aerodynamic loads were discretely distributed along the wing by computing the equivalent lift force  
 278 and pitching moment components at rib boundary locations at 25% of the local chord length. They were  
 279 introduced to the wingbox finite element model by means of multipoint constraint (MPC) non-stiffening  
 280 rigid body elements (RBE3) in the rib's perimeter nodes. Spring elements (CEALS1) combined with  
 281 RBE2 elements were used to create realistic boundary conditions at the wingbox root at the aircraft  
 282 centerline. The spring elements were attached to a fixed ground point. The translational and rotational  
 283 stiffness properties were selected to result in end boundary conditions sufficiently close to the clamped  
 284 case, due to the lack of available data on wingbox root stiffness values for real aircraft structures in the  
 285 open literature. The wingbox finite element models have been verified by numerous quality pre-analysis  
 286 checks, including element free edge, mesh and element quality, boundary conditions, coincident nodes,  
 287 material and element properties, and element normal. Finite element model checks help to safeguard  
 288 against fundamental errors, and also guard against the frustration associated with having the solver run for  
 289 a considerable amount of time, only to abort due to incorrect or missing data.

#### 290 4. Structural design optimization of the CRM wingbox

291 Structural optimization methods evolved in the aerospace industry in the late 1950s, when the need to  
292 design lightweight structures was critical [32,33,34]. Since then, the aerospace manufacturing industry  
293 has shown increasing interest in the application of optimization methods for the optimum design of  
294 minimum-weight aircraft structural components [35,36,37]. The survey paper by Venkayya [38] presents  
295 an exhaustive review of relevant literature on the structural optimization of aerospace structures. In their  
296 work Wang et al. [39] offer numerous and important references on the applications of design optimization  
297 approaches to the field of aerospace structure engineering. The CRM wingbox structural optimization that  
298 is presented in this work purposely deals with property optimization. Therefore, the locations of the ribs,  
299 stiffeners and spars are considered invariable and shape optimization is not performed in this study. The  
300 optimization is performed using the commercially available off-the-shelf MSC Nastran gradient-based  
301 Sol 200 optimizer [40] which is widely used and recognized by the aerospace industry across the globe.  
302 One of the key advantages underlying the selection of gradient-based algorithms is their effectiveness in  
303 solving optimization problems where the design space is significantly large, and where the number of  
304 design variables is therefore considerably greater than the number of objectives and constraints. Another  
305 advantage is their relative computational efficiency due to rapid convergence rates with clear convergence  
306 criteria. However, one of the main drawbacks of gradient-based methods is the presence of multiple local  
307 optima, resulting in solutions where global optimality cannot be easily guaranteed. In gradient-based  
308 methods, global optimality is sought by randomly searching the design space from different starting  
309 points. In practice, one normally seeks procedures through which the design search space is explored in a  
310 cost-effective manner, aiming for a better optimal solution within an acceptable level of accuracy  
311 depending on the size and nature of the optimization problem. For this reason a practical design  
312 optimization procedure using gradient-based methods was utilized for the structural sizing for both  
313 metallic and composite configuration in order to calculate the mass of the CRM primary wing structure in  
314 an effective and efficient way. The reader may wish to refer to the work of Dababneh et al. [41] for more  
315 details regarding the practical design optimization framework.

##### 316 4.1 Structural layout of the CRM wingbox models used for structural optimization

317 The load-carrying structure of NASA's Common Research Model transport aircraft wing  
318 configuration is used for the optimization. Four different wingbox models of increasing structural  
319 complexity were created as part of this study. The structural layout of the CRM wingbox models is given  
320 in Fig. 11. These models are discretized into components which act as design optimization zones along  
321 the span. These areas include the upper and lower skins, front and rear spar webs, ribs, spar caps and  
322 stiffeners. Model 1 contains 168 design zones. Model 2 contains 210 design zones. Model 3 contains 378  
323 design zones. Model 4 contains 1,870 design zones. The chordwise design zones are prescribed by the  
324 stringer pitch, while in the spanwise direction the design zones are limited by the rib spacing. In the finite  
325 element model, each design field consists of a number of finite elements that all comprise the same  
326 thicknesses/cross-sectional areas and stiffness properties.

327

328

329

330

331

332

333

334

335

336

337

338

339

340

341

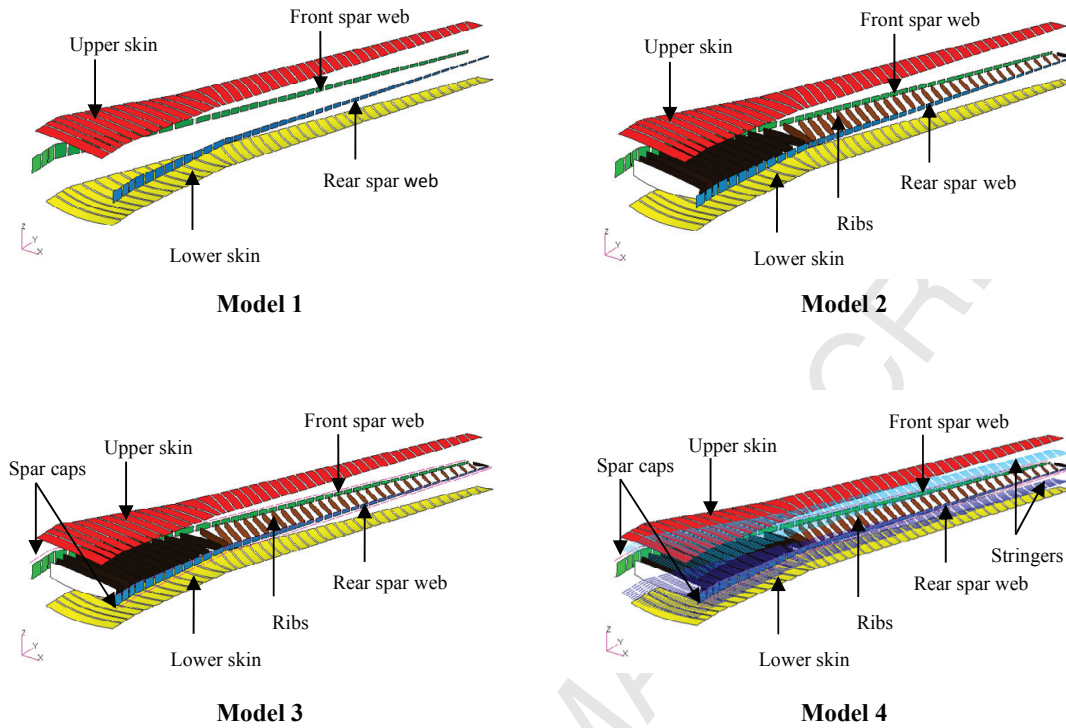


Fig. 11 Design optimization zones of CRM wingbox-Models 1-4

#### 4.2 Formulation of the CRM wingbox optimization problem

During this study, it was decided to formulate this optimization problem in a simple way as possible, in order to stay focused on the main objective and ensure a thorough understanding of the decisions made, including how to solve or eliminate any unusual situations that may arise during the solution process. The masses of the metallic and composite configurations of the CRM wingbox were minimized when subjected to static strength/stiffness constraints on the design variables. The optimization problem mathematically formulated in terms of the objective function, design variables and imposed constraints as follows:

##### 1. Objective function

The objective function is the structural mass of the CRM wingbox. The objective function can be represented by:

$$\text{minimize } M(\mathbf{x}), \text{ where } M(\mathbf{x}) \text{ is the structural mass of the CRM wingbox} \quad (1)$$

##### 2. Design variables

For the optimization problem, considering the wingbox construction material to be a metallic material, one design variable per design field is defined. The design variables include the thicknesses of the wingbox skins, spar webs and ribs, as well as the cross-sectional areas of the wingbox spar caps and

357 stiffeners. A minimum gauge thickness of 2 mm and a cross-sectional area of 144 mm<sup>2</sup> are specified for  
358 the design variables. The limits on the design variables are defined as follows:

$$2.0 \leq t_{metallic} \quad (2)$$

$$144.0 \leq a_{metallic} \quad (3)$$

359 On the other hand, considering the wingbox construction material to be a composite material, the  
360 corresponding design variables for the wingbox skins, spar webs and ribs are the thicknesses of each ply  
361 or lamina in the composite laminate associated with each design field. The cross-sectional areas of the  
362 composite spar caps and stiffeners are also treated as individual design variables for each design zone.  
363 The minimum ply thickness is taken to be 0.127 mm; while a 3 mm minimum gauge laminate thickness is  
364 recommended to maintain an adequate level of laminate damage tolerance. The laminate ply thicknesses  
365 are treated as individual design variables and a count is made of the required number of plies in each ply  
366 orientation angle. The limits on the number of plies in each ply orientation angle are given as

$$3 \leq n_{ply} \quad (4)$$

367 Minimum cross-sectional areas of 216 mm<sup>2</sup> for the composite spar caps and stiffeners are specified  
368 and the limits on the design variables are defined as

$$216.0 \leq a_{composite} \quad (5)$$

369 3. Static strength design constraints

370 For metallic skin panels, spar webs and ribs, the von Mises stress is checked against the material  
371 allowable stress as defined in the following equation:

$$\sigma_{von\ Mises} \leq \sigma_{allowable} \quad (6)$$

372 For composite skin panels, spar webs and ribs, the Tsai-Wu criterion [42,43,44] is used to predict the  
373 strength of the composite laminate in terms of the failure index (*FI*). For orthotropic plate analysis, under  
374 the plane stress state, the Tsai-Wu strength theory predicts that a lamina will undergo failure when the  
375 following inequality is satisfied:

$$FI = F_1\sigma_1 + F_2\sigma_2 + F_{11}\sigma_1^2 + 2F_{12}\sigma_1\sigma_2 + F_{22}\sigma_2^2 + F_{66}\sigma_6^2 \geq 1. \quad (7)$$

376 The coefficients  $F_1$ - $F_{66}$ , with the exception of  $F_{12}$ , are described in terms of strengths in the principal  
377 material directions.  $F_{12}$  accounts for the interaction between normal stresses,  $\sigma_1$  and  $\sigma_2$ .

378 The principal strains in each ply are also checked against the material allowable strain to ensure the  
379 integrity of the plies and failure-free laminates. The allowable strain value of 3500  $\mu\epsilon$  includes the  
380 margins due to fatigue and damage tolerance, assuming that the allowable strains are identical in terms of  
381 tension and compression. Thus, the following constraint is placed on the strain value used for sizing the  
382 structure:

$$\varepsilon_{principal} \leq \varepsilon_{allowable} \quad (8)$$

383 The spar caps and the longitudinal stiffeners are designed to carry axial stress only. Therefore, they  
 384 are designed according to their stress state against the allowable stress of the material as defined in the  
 385 following equation:

$$\sigma_{axial} \leq \sigma_{allowable} \quad (9)$$

386 4. Static stiffness constraints

387 The flexural stiffness of the wingbox is controlled by limiting the vertical displacement of the wingtip  
 388 leading edge [45,46]. The wingtip deflection  $\delta_{tip(z)}$  for the CRM wing at a 2.5g pull-up maneuver is  
 389 assumed to be 15% of the wing semi-span  $b$ .

$$\delta_{tip(z)} \leq 15\% \cdot b \quad (10)$$

390 The torsional stiffness, which is necessary to counteract the twisting of the wing under aerodynamic  
 391 loads and thus prevents flutter, is controlled by constraining the twist angle at the tip chord of the wing.  
 392 The angular deformation at the wingtip chord is constrained by limiting it to a value of  $6^\circ$  to ensure  
 393 sufficient torsional stiffness and thus an adequate aeroelastic response [43]. The twist angle constraint is  
 394 defined using the vertical displacements at the wingtip chord ends. Equation (11) shows that the twist  
 395 angle at the wingtip should not exceed  $6^\circ$ .  $(\delta)_{max}^+$  and  $(\delta)_{max}^-$  are the maximum vertical displacements in  
 396 positive and negative directions of the z-coordinate, respectively. Here,  $C$  is the wing chord length at the  
 397 required location:

$$\theta_{tip} \leq 6^\circ, \text{ where } \theta = \arctan\left(\frac{(\delta)_{max}^+ - (\delta)_{max}^-}{C}\right) \quad (11)$$

#### 398 4.3 Optimization results of the metallic and composite CRM wingbox models

399 The CRM wingbox was optimized to meet static strength and stiffness requirements subject to lift  
 400 force only. In this initial study, no aeroelastic or manufacturing constraints are imposed nor any other  
 401 types of aerodynamic or inertial forces included, keeping the problem simple and focusing on the effects  
 402 of using different structural wingbox models for the structural optimization. Moreover, all the design  
 403 variables for this problem were treated as continuous design variables. The gradient-based optimization  
 404 algorithm, DOT, was used for the design sizing of the CRM metallic and composite wingbox models.  
 405 During this initial stage, it was decided to formulate this optimization study in a simple way as possible,  
 406 in order to stay focused on the main objective and ensure a thorough understanding of the decisions made,  
 407 including how to solve or eliminate any unusual situations that may arise during the solution process. In  
 408 the optimization process, the design variables change continuously within a range between a lower limit  
 409 and an unbounded upper limit. Therefore, the thicknesses and cross-sectional areas of the wingbox model  
 410 structural components are allowed to vary until all the design requirements are met. During the  
 411 optimization, convergence is aimed for by using different starting values for the design variables, and the  
 412 effects of these starting values on the final optimization are investigated. The sets of initial values for the  
 413 design variables, the thin panel thicknesses, the number of plies in each ply orientation and the flange

414 cross-sectional areas, for both the metallic and composite CRM wingbox optimization models, are  
 415 specified as follows:

$$t_{metallic} = \{2, 4, 6, 10, 13\} \text{ mm}, \quad (12)$$

$$n_{ply} = \{3, 4, 8, 11, 15\}, \quad (13)$$

$$a_{metallic} = \{144, 215, 420, 643, 858\} \text{ mm}^2, \quad (14)$$

$$a_{composite} = \{218, 258, 358, 585, 858\} \text{ mm}^2. \quad (15)$$

416 Tables 1 and 2 show the optimized masses of the metallic and composite CRM wingbox models,  
 417 respectively, using the sets of initial values for the design variables. Based on the results, it can be seen  
 418 that by using different initial guesses for the design variables, various local optimum designs can be  
 419 obtained from the gradient-based optimization solution. In all the solutions, convergence is achieved and  
 420 the bold values in the tables denote the local minimum solutions obtained for each CRM wingbox model.

421 **Table 1** Optimized masses of metallic CRM wingbox models (kg)

Design variables and initial values				
$t_1 a_1$	$t_2 a_2$	$t_3 a_3$	$t_4 a_4$	$t_5 a_5$
Wingbox Model 1				
<b>17,990</b>	18,587	18,641	18,531	17,999
Wingbox Model 2				
12,167	12,271	12,166	<b>12,149</b>	12,157
Wingbox Model 3				
12,245	12,129	12,167	12,276	<b>12,116</b>
Wingbox Model 4				
12,276	<b>12,272</b>	12,325	12,445	12,401

422

423 **Table 2** Optimized masses of composite CRM wingbox models (kg)

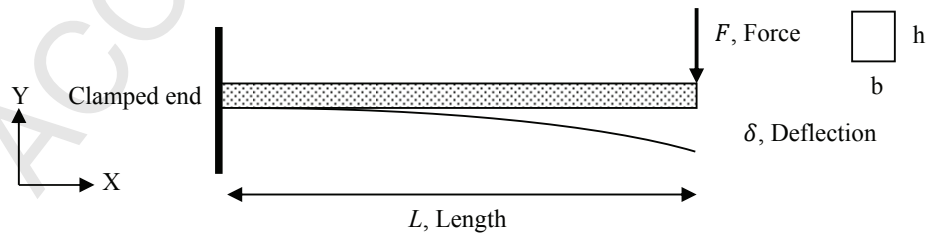
Design variables and initial values				
$n_{ply1} a_1$	$n_{ply2} a_2$	$n_{ply3} a_3$	$n_{ply4} a_4$	$n_{ply5} a_5$
Wingbox Model 1				
<b>12,862</b>	13,468	13,449	13,461	13,514
Wingbox Model 2				
8,535	9,070	9,355	<b>8,321</b>	8,587
Wingbox Model 3				
8,373	8,269	9,093	9,058	<b>7,891</b>
Wingbox Model 4				
8,917	7,940	<b>7,192</b>	8,367	7,366

424 The optimized masses of the second, third and fourth wingbox models; turned out to be lower than  
 425 those obtained by the use of the first wingbox model. Therefore, it can be seen that, in the context of using  
 426 high-fidelity structural models to describe and represent the CRM wingbox design, these models attempt  
 427 to improve the optimized masses of the wingbox. This representation of the CRM wingbox increases the  
 428 number of structural elements describing the wingbox from one model to the next. Thus, the number of  
 429 design variables increases and the design space becomes larger. The possible design alternatives within  
 430 the design domain thus increase, thereby increasing the chances of arriving at a better local optimum  
 431 solution and mass estimate.

432 The optimized masses of the composite wingbox models indicate that the results are more sensitive to  
 433 their initial starting values for the design variables than the results of the metallic wingbox models. In this  
 434 case, there is a greater difference in the optimized masses between the composite wingbox models than  
 435 for the metallic wingbox models. This behavior can be explained by the different mechanical properties  
 436 of the composite laminate, which are more complex than those of the metallic material. The global  
 437 laminate properties are dependent on the fiber orientation angles, the number of layers and their  
 438 thicknesses, and the stacking sequence. For an orthotropic material, at least two elastic constants are  
 439 needed to describe the stress-strain behavior in the material. Therefore, the stiffness of an orthotropic  
 440 plate must be described by two values, one along the longitudinal direction of the fibers, commonly  
 441 referred to as  $E_L$ , and one transverse to the direction of the fibers, usually denoted by  $E_T$ . Using classical  
 442 lamination theory [42,43,44], the bending stiffness matrix of the symmetric laminate  $[D]$  can be written  
 443 as

$$[D] = \frac{2}{3} \sum_{k=1}^{n_{ply}} [\bar{Q}]_k (Z_k^3 - Z_{k+1}^3), \quad (16)$$

444 where  $[\bar{Q}]_k$  is the transformed reduced stiffness matrix of the  $k$ th layer,  $(Z_k - Z_{k+1})$  is the ply thickness  
 445 and  $n_{ply}$  is the number of plies. The transformed reduced stiffness matrix can be defined in terms of the  
 446 ply angle  $\phi$  and the elastic constants  $E_{11}$ ,  $E_{22}$ ,  $\nu_{12}$  and  $G_{12}$  of the orthotropic layer. The mathematical  
 447 derivation of  $[\bar{Q}]_k$  can be found in [42,43]. On the other hand, the bending stiffness  $k_b$  of beam-like  
 448 metallic structures under an applied force  $F$  [48,49], as shown in Fig. 12, can be defined as



454 **Fig. 12** Deflection of cantilevered beam

$$k_b = \frac{F}{\delta} = \frac{3EI_{xx}}{L^3}, \text{ where } I_{xx} = \frac{1}{12}bh^3, E \text{ is Young's Modulus.} \quad (17)$$

455 Mathematically, the area moment of inertia  $I_{xx}$  appears in the numerator of the stiffness equation,  
 456 Eqn. (17), therefore the larger the area moment of the inertia, the less the structure deflects and thus the  
 457 greater the stiffness. According to Eqns. (16) and (17), the derivation of the composite laminate bending  
 458 stiffness with respect to the layer thickness is a bit more complex than for the metallic isotropic material,  
 459 where the stiffness is described by one constant value; the modulus  $E$  of the material regardless of the  
 460 direction of load. An infinitesimal change in the composite layer thickness has an influence on its own  
 461 stiffness and on the stiffness of all the layers above. We can therefore create an equivalent design with the  
 462 same bending stiffness by changing the thicknesses of the composite layers while preserving the original  
 463 ply orientation of each layer and the same total thickness of the laminate. The existence of multiple  
 464 laminate equivalent designs has important implications for the optimization process, in that it results in  
 465 multiple optima and will always have a major influence on the objective function value.

466 The accuracy of the four proposed wingbox models in predicting the mass of the primary wing  
 467 structure is analyzed using the estimated optimum mass of the fourth wingbox model  $m_4$  as a reference  
 468 value. Table 3 shows the errors of the wingbox masses predicted using the four different models of  
 469 increasing structural complexity. The error has been calculated as

470

**Table 3** Errors of the wingbox mass estimation

Wingbox Model	Metallic [%]	Composite [%]
Model 1	31.78	44.08
Model 2	-1.01	13.57
Model 3	-1.29	8.86
Model 4	0.00	0.00

471

472 From Table 3, it is observed that the first wingbox model over predicts the primary wing structure  
 473 mass for the CRM aircraft in comparison with the other models. A possible cause for this larger deviation  
 474 of Model 1 can be explained by the lack of internal chordwise oriented wing structural elements, meaning  
 475 that the wing skins have to carry an additional part of the lift load that is usually transferred to the wing  
 476 main spar by the ribs. Furthermore, the first wingbox model is a hollow beam and is less efficient than the  
 477 rest of the models, which contain ribs with hybrid orientation, in torsional stiffness. As a consequence, the  
 478 wingbox skin thicknesses are increased, resulting in an increase in the mass of the wingbox. From the  
 479 results summarized in Table 3, it can be seen that the second and third metallic wingbox models show  
 480 good accuracy with errors of -1.01 and -1.29%, respectively, for the mass estimation of the CRM  
 481 wingbox. For the composite wingbox models, this is not the case. The second and third composite  
 482 wingbox models over predict the primary wing structure mass for the CRM aircraft with errors of 13.57  
 483 and 8.86%, respectively.

484 The total wall-clock time for each optimization run until convergence occurs and an optimum solution  
 485 has been found is also compared, and the summary of the computational time is shown in Table 4. In this  
 486 study, computations were carried out on a laptop computer with a 2.60 GHz Intel i5 CPU and 8GB RAM.  
 487 From the results given in Table 4, it can be seen that the computational times for the optimized composite

488 models are very long compared to the optimized metallic models, as the design space for the composite  
 489 models is relatively complex with a large number of design variables and constraints. Furthermore, it is  
 490 also observed that the optimization run time was significantly increased for the fourth wingbox mass  
 491 estimation model for both the metallic and composite CRM wingbox configurations. Despite the long run  
 492 time, the fourth wingbox model is shown to have improved the accuracy of the objective function value,  
 493 particularly for the CRM composite wingbox model, as explained in the foregoing discussion of the  
 494 results presented in Table 3.

495 **Table 4** Total wall-clock time (seconds)

Wingbox Model	Metallic [s]	Composite [s]
Model 1	55.5	562.6
Model 2	55.9	497.1
Model 3	63.9	662.9
Model 4	742.4	5,303.4

496  
 497 The values of the CRM wingbox mass obtained in the current study are compared with the estimated  
 498 mass values according to the open scientific literature. It should be noted that no mass values were  
 499 reported for the composite CRM wingbox in the literature. Generally, the wingbox mass value of the  
 500 metallic CRM wing calculated in the current study is in good agreement with the value estimated  
 501 (12,263kg) by Kenway et al. [50]. On the other hand, the CRM wingbox mass (11,494 kg) calculated by  
 502 Klimmek [51] is lower than the mass reported in the current study. Possible sources for discrepancies can  
 503 be traced to the location of the spars and the number of ribs, as well as their spacing and location, which  
 504 have a direct effect on the wingbox mass. Flight conditions for the calculation of sizing loads and/or  
 505 aerodynamic loads, the definition and number of design variables and constraints in the scenario of using  
 506 optimization techniques.

## 507 5. Concluding remarks

508 Based on the results presented in Tables 1 and 2 in this study, the following points could be  
 509 concluded:

- 510 • In a scenario where high-fidelity structural models are used to describe and represent the CRM  
 511 wingbox model, these models do indeed attempt to improve the optimized masses of the wingbox.  
 512 This representation of the CRM wingbox increases the number of structural elements describing  
 513 the wingbox from one model to the next. Thus, the number of design variables increases, and the  
 514 design space enlarges. The possible design alternatives within the design domain then increase,  
 515 which in turn increases the chances of arriving at a better local optimum solution and mass  
 516 estimate.
- 517 • The mass of the metallic CRM wing box can be estimated with an acceptable level of accuracy and  
 518 reduced computational time with high degree of confidence by using the second wingbox model of  
 519 structural fidelity, as long as the gradient-based designs are also optimized using a sufficient

520 number of different starting values for the design variables, as practiced in the design and  
521 optimization phase of this study (See Table 1).

522 • In the scenario where composite materials are used as the primary construction material for the  
523 design of the CRM wingbox, it is observed that by increasing the structural fidelity of the wingbox  
524 model, as observed in the second and third wingbox models, the discrepancy in the mass estimate  
525 becomes smaller but still significant. Therefore, it is strongly recommended that the fourth  
526 wingbox model be used as the baseline model for the preliminary estimate of the composite CRM  
527 wingbox mass, requiring higher computational time in order to achieve the required accuracy  
528 level.

529 • The optimized masses of the composite wingbox models indicate that the results are more  
530 sensitive to the initial starting values of the design variables than to the results of the metallic  
531 wingbox models (See Table 1 and 2). In this case, the change in the optimized masses of the  
532 composite wingbox models is larger than the change for the metallic wingbox. This behavior can  
533 be explained by the different mechanical properties of the composite laminate, which are more  
534 complex than those of metallic structures. The computational times for the optimized composite  
535 models are long and the design space is relatively complex, with a large number of design  
536 variables and constraints compared to the optimized metallic models.

## 537 6. Future work

538 In the view of the above, and for a more detailed insight into the CRM wingbox mass estimation,  
539 further studies that will account for the effects of considering aeroelasticity, buckling, fatigue and damage  
540 tolerance, manufacturing requirements, and inertial forces will be considered using multidisciplinary  
541 design optimization technique. This will aim to achieve a better understanding of the actual wingbox  
542 structural material distributions in terms of thickness and orientation, and finally to assess the structural  
543 behavior of the wing, including global displacement and local stresses. This will be a rather appropriate  
544 view compared to that from an industrial design perspective.

## 545 References

546 [1] Raymer, D. P. (2006). *Aircraft Design: A Conceptual Approach* (4th ed.). Washington, USA:  
547 AIAA Education Series.

548 [2] Roskam, J. (1989). *Airplane Design: Part III - Layout Design of Cockpit, Fuselage, Wing and*  
549 *Empennage: Cutaways and Inboard Profiles*. Kansas: Roskam Aviation and Engineering  
550 Corporation.

551 [3] Torenbeek, E. (1982). *Synthesis of Subsonic Airplane Design*. Amsterdam: Delft University Press.

552 [4] Ediger, K., Zeumer, C., & Dugas, M. (2004). *FAME-liA 4.00 F3 - Validation Document*. Technical  
553 Report, Airbus Deutschland GmbH.

- 554 [5] Klimmek, T. (2014). Parametric Set-Up of a Structural Model for FERMAT Configuration for  
555 Aeroelastic and Loads Analysis. *ASDJournal*, 3, (2), 31-49.
- 556 [6] Jutte, C. V., Stanford, B. K., & Wieseman, C. D. (2015). *Internal Structural Design of the*  
557 *Common Research Model Wing Box for Aeroelastic Tailoring*. Hampton, Virginia: NASA.
- 558 [7] Murphy, N. (1987). *Analytical Wing Weight Prediction/Estimation Using Computer Based Design*  
559 *Techniques*. PhD Thesis, Cranfield Institute of Technology.
- 560 [8] Ardema, M., Chambers, M., Patron, A., Hahn, A., Miura, H., & Moore, M. (1996). *Analytical*  
561 *Fuselage and Wing Weight Estimation of Transport Aircraft*. NASA.
- 562 [9] Kundu, A. (2010). *Aircraft Design*. Cambridge: Cambridge University Press.
- 563 [10] Elham, A. (2013). *Weight Indexing for Multidisciplinary Design Optimization of Lifting Surfaces*.  
564 PhD Thesis, Delft University of Technology.
- 565 [11] Howe, D. (2000). *Aircraft Conceptual Design Synthesis*. London: Professional Engineering  
566 Publishing Limited London and Bury St Edmunds.
- 567 [12] Dababneh, O and Kipouros, T (2018). A review of aircraft wing mass estimation methods.  
568 *Aerospace Science and Technology*, 72, 256-266.
- 569 [13] Droegkamp, M. (1992). Finite Element Model Weight Estimation. SAWE Paper No. 2089, *51st*  
570 *Annual Conference*. Hartford, Connecticut: Society of Allied Weight Engineers, Inc.
- 571 [14] Zaidel, S. J. (1992). A-12 Structural Target Weight Distribution Using the Finite Element Model  
572 (FEM). SAWE Paper No. 2110, *51st Annual Conference*. Hartford, Connecticut: Society of  
573 Allied Weight Engineers, Inc.
- 574 [15] Mitchell, P. M. (1993). Advanced Finite Element Weight Estimation Process on the High Speed  
575 Civil Transport. SAWE Paper No. 2169, *52nd Annual Conference*. Biloxi, Mississippi: Society of  
576 Allied Weight Engineers, Inc.
- 577 [16] Wenzel, J., Sinapius, U., & Gabbert, U. (2012). Primary Structure Mass Estimation in Early  
578 Phases of Aircraft Development using the Finite Element Method. *CEAS Aeronautical Journal*, 3  
579 (1), 35-44.
- 580 [17] Dababneh, O., & Kayran, A. (2014). Design, analysis and optimization of thin walled semi-  
581 monocoque wing structures using different structural idealization in the preliminary design phase.  
582 *International Journal of Structural Integrity*, 5 (3), 214-226.
- 583 [18] Bindolino, G., Ghiringhelli, G., Ricci, S., & Terraneo, M. (2010). Multilevel Structural  
584 Optimization for Preliminary Wing-Box Weight. *Journal of Aircraft*, 47, No. 2, 475-489.

- 585 [19] Hurlimann, F., Kelm, R., Dugas, M., Oltmann, K., & Kress, G. (2010). Mass estimation of  
586 transport aircraft wingbox structures with a CAD/CAE-based multidisciplinary process. *Aerospace*  
587 *Science and Technology*, 15 (4), 323-333.
- 588 [20] Dorbath, F., Nagel, B., & Gollnick, V. (2012). A Knowledge Based Approach for Extended  
589 Physics-Based Wing Mass Estimation in early Design Stages. *28th Congress of the International*  
590 *Council of the Aeronautical Sciences*. 6. Brisbane: ICAS.
- 591 [21] Holden, C. M., & Keane, A. J. (2004). Visualization Methodologies in Aircraft Design. AIAA-  
592 2004-4449. *10th AIAA/ISSMO Multidisciplinary Analysis and Optimization Conference*. Albany,  
593 New York.
- 594 [22] Ciampa, P. M., Nagel, B., & Tooren, M. (2010). Global Local Structural Optimization of  
595 Transportation Aircraft Wings. AIAA 2010-3098. *51st AIAA/ASME/ASCE/AHS/ASC Structures,*  
596 *Structural Dynamics, and Materials Conference*. Orlando, Florida: AIAA.
- 597 [23] Yang, Y., Wu, Z., & Yang, C. (2012). Equivalent Plate Modeling for Complex Wing  
598 Configurations. *Procedia Engineering*, 31, 409-415.
- 599 [24] Ritter, M., & Cesnik, C. (2016). Large Deformation Modeling of a Beam Type Structure and a 3D  
600 Wingbox using an Enhanced Modal Approach. AIAA 2016-1708. *57th*  
601 *AIAA/ASME/ASCE/AHS/ASC Structures, Structural Dynamics, and Materials Conference*. San  
602 Diego, California: AIAA.
- 603 [25] Werter, N., & Breuker, R. (2015). Aeroelastic tailoring and structural optimization using an  
604 advanced dynamic aeroelastic framework. *IFASD 2015: 16th International Forum on*  
605 *Aeroelasticity and Structural Dynamics Conference*. Saint Petersburg, Russia.
- 606 [26] EASA. (2015). *Certification Specifications and Acceptable Means of Compliance for Large*  
607 *Aeroplanes CS-25, Amendment 16*. Retrieved March 28, 2015, from  
608 [http://easa.europa.eu/system/files/dfu/CS-25\\_20Amdendment\\_16.pdf](http://easa.europa.eu/system/files/dfu/CS-25_20Amdendment_16.pdf)
- 609 [27] FAA. *FAR 25, Airworthiness Standards: Transport Category Airplanes (Title 14 CFR Part 25)*.  
610 Retrieved January 15, 2014, from [http://flightsimulation.com/data/FARS/part\\_25.html](http://flightsimulation.com/data/FARS/part_25.html)
- 611 [28] ASM. (1978). *ASM Aerospace Specification Metals, Aluminum 7050-T7451*. Retrieved June 12,  
612 2014, from <http://asm.matweb.com/search/SpecificMaterial.asp?bassnum=MA7050T745>
- 613 [29] ASM. (1978). *ASM Aerospace Specification Metals, Aluminum 2024-T3*. Retrieved June 12, 2014,  
614 from <http://asm.matweb.com/search/SpecificMaterial.asp?bassnum=%20MA2024T3>

- 615 [30] Soni, S. R. (1980). *Elastic Properties of T300/5208 Bidirectional Symmetric Laminates -*  
616 *Technical Report Afwal-Tr-80-4111*. Ohio 45433: Materials Laboratory - Air Force Wright  
617 Aeronautical Laboratories - Air Force Systems Command.
- 618 [31] ESDU. (1999). *Computer program for estimation of spanwise loading of wings with camber and*  
619 *twist in subsonic attached flow. Lifting-surface theory*. Retrieved March 12, 2014, from  
620 [https://www.esdu.com/cgi-bin/ps.pl?sess=cranfield5\\_1160220142018cql&t=doc&p=esdu\\_95010c](https://www.esdu.com/cgi-bin/ps.pl?sess=cranfield5_1160220142018cql&t=doc&p=esdu_95010c)
- 621 [32] Brennan, J. (1999). Integrating Optimization into the Design Process. *Proceedings of the Altair*  
622 *HyperWorks Technology Showcase*. London.
- 623 [33] Cervellera, P. (2004). Optimization Driven Design Process: Practical Experience on Structural  
624 Components. *Proceedings of the 14th Convegno Nazionae ADM*. Bari.
- 625 [34] Gartmeier, O., & Dunne, W. L. (1999). Structural Optimization in Vehicle Design Development.  
626 *MSC Worldwide Automotive Conference*.
- 627 [35] Krog, L., Tucker, A., & Rollema, G. (2002). Application of Topology, Sizing and Shape  
628 Optimization Methods to Optimal Design of Aircraft Components. *3rd Altair UK HyperWorks*  
629 *Users Conference*.
- 630 [36] Krog, L., Tucker, A., Kempt, M., & Boyd, R. (2004). Topology Optimization of Aircraft Wing  
631 Box Ribs, AIAA-2004-4481. *Proc. 10th AIAA/ISSMO Symposium on Multidisciplinary Analysis*  
632 *and Optimization*. Albany, NY.
- 633 [37] Schumacher, G., Stettner, M., Zotemantel, R., O'Leary, O., & Wagner, M. (2004). Optimization  
634 Assisted Structural Design of New Military Transport Aircraft, AIAA-2004-4641. *Proc. 10th*  
635 *AIAA MAO Conference*. Albany, NY.
- 636 [38] Venkayya, V. B. (1971). Design of Optimum Structures. *Computers and Structures* (No.1), 265-  
637 309.
- 638 [39] Wang, Z., Huang, W. & Yan, L. (2014). Multidisciplinary design optimization approach and its  
639 application to aerospace engineering. *Chinese Science Bulletin*, 59, (36), 5338-5353
- 640 [40] MSC Nastran (2012). *Design Sensitivity and Optimization User's Guide*. Santa Ana, CA:  
641 MSC Software Corporation.
- 642 [41] Dababneh O, Kipouros T & Whidborne JF (2018). Application of an efficient gradient-based  
643 optimization strategy for aircraft wing structures, *Aerospace*, 5, (1), 1-27.
- 644 [42] Jones, R. M. (1999). *Mechanics of Composite Materials* (2nd ed.). Taylor & Francis.

- 645 [43] Tsai, S. W., & Hahn, H. T. (1980). *Introduction to Composite Materials*. Technomic Publishing  
646 Co.
- 647 [44] Kassapoglou, C. (2013). *Review of Laminate Strength and Failure Criteria, in Design and*  
648 *Analysis of Composite Structures: With Applications to Aerospace Structures*. Oxford: John Wiley  
649 & Sons Ltd.
- 650 [45] Starnes Jr, J. R., & Haftka, R. T. (1979). Preliminary Design of Composite Wings for Buckling,  
651 Stress and Displacement Constraints. *Journal of Aircraft*, 16 (8), 564-570.
- 652 [46] Oliver, M., climent, H., & Rosich, F. (1999). Non Linear Effects of Applied Loads and Large  
653 Deformations on Aircraft Normal Modes. *RTO AVT Specialists' Meeting on Structural Aspects of*  
654 *Flexible Aircraft Control*. Ottawa.
- 655 [47] Liu, Q., Mulani, S., & Kapani, R. K. (2014). Global/Local Multidisciplinary Design Optimization  
656 of Subsonic Wing, AIAA 2014-0471. *10th AIAA Multidisciplinary Design Optimization*  
657 *Conference - AIAA SciTech*. National Harbor, Maryland: AIAA, Inc.
- 658 [48] Niu, M. C. (1999). *Airframe Stress Analysis and Sizing*. Conmilit Pres Ltd.
- 659 [49] Beer, F., Johnston, J. E., DeWolf, J., & Mazurek, D. (2014). *Mechanics of Materials* (7th ed.).  
660 McGraw-Hill Education.
- 661 [50] Kenway, G. K., Martins, J. R., & Kennedy, G. J. (2014). Aerostructural optimization of the  
662 Common Research Model configuration, AIAA 2014-3274. *15th AIAA/ISSMO Multidisciplinary*  
663 *Analysis and Optimization Conference*. Atlanta, GA: AIAA Aviation.
- 664 [51] Klimmek, T. (2014). Parametric Set-Up of a Structural Model for FERMAT Configuration for  
665 Aeroelastic and Loads Analysis. *ASDJournal*, 3, (2), 31-49.

# Influence of high fidelity structural models on the predicted mass of aircraft wing using design optimization

Dababneh, Odeh

2018-05-26

Attribution-NonCommercial-NoDerivatives 4.0 International

---

Odeh Dababneh and Timoleon Kipouros. Influence of high fidelity structural models on the predicted mass of aircraft wing using design optimization. *Aerospace Science and Technology*, Volume 79, August 2018, Pages 164-173

<https://doi.org/10.1016/j.ast.2018.05.043>

*Downloaded from CERES Research Repository, Cranfield University*